Discrete time crystal in globally driven interacting quantum systems without disorder

Wing Chi Yu,[1,*] Jirawat Tangpanitanon,[1,†] Alexander W. Glaetzle,[1,2] Dieter Jaksch,[2,1] and Dimitris G. Angelakis[1,3,‡]

[1]*Centre for Quantum Technologies, National University of Singapore, 3 Science Drive 2, Singapore 117543, Singapore*

[2]*Clarendon Laboratory, University of Oxford, Parks Road, Oxford OX1 3PU, United Kingdom*

[3]*School of Electronic and Computer Engineering, Technical University of Crete, Chania, Crete 73100, Greece*

(Received 8 November 2018; published 25 March 2019)

Time crystals in periodically driven systems have initially been studied assuming either the ability to quench the Hamiltonian between different many-body regimes, the presence of disorder or long-range interactions. Here we propose the simplest scheme to observe discrete time crystal dynamics in a one-dimensional driven quantum system of the Ising type with short-range interactions and no disorder. The system is subject only to a periodic kick by a global magnetic field, and no extra Hamiltonian quenching is performed. We analyze the emerging time crystal stabilizing mechanisms via extensive numerics as well as using an analytic approach based on an off-resonant transition model. Due to the simplicity of the driven Ising model, our proposal can be implemented with current experimental platforms including trapped ions, Rydberg atoms, and superconducting circuits.

DOI: 10.1103/PhysRevA.99.033618

I. INTRODUCTION

In 2012, Wilczek proposed the idea of quantum time crystals which spontaneously break the continuous time translation symmetry [1]. He suggested that a ring of interacting bosons prepared in the ground state can switch to a periodic motion in time if the magnetic flux through the ring is properly chosen. However, a no-go theorem later pointed out that such a time crystal phase is forbidden in equilibrium [2,3]. Alternatively, Sacha first proposed to search for time crystal dynamics in periodically driven systems [4] which was further concretized by Khemani *et al.* [5] and Else *et al.* [6], respectively, studying many-body models. In the presence of strong disorder, the system is many-body localized (MBL) and does not absorb heat from the drive. In this MBL regime, the system can oscillate with a period which is different from the drive's without thermalizing to an infinite temperature. Such a phase is known as a discrete (or Floquet) time crystal (DTC) to emphasize the discreteness and to differentiate from the original proposal by Wilczek. Subsequent theoretical and numerical studies have demonstrated the existence of DTC in various disordered Floquet systems [7–10].

Recently, DTCs have been observed in various experiments with trapped ions [11], spatial crystals ammonium dihydrogen phosphate $NH_4H_2PO_4$ [12,13], and nitrogen-vacancy centers in diamond [14] in the presence of disorder or long-range interactions. While in Ref. [11], DTCs were realized in the MBL phase, the disorder in Refs. [12–14] was insufficient for reaching the MBL regime. This triggered a search for DTCs that are not protected by MBL [15–24]. Driven many-body systems without disorder that exhibit a DTC have been proposed for quenched Hamiltonian with short-range interactions in cold atoms [22], in two dimensions or higher [19], in the regime with all-to-all spin interactions [23], and ultracold atoms bouncing on an oscillating atom mirror [24].

In this work, we study a DTC in a simple periodically driven one-dimensional Ising quantum chains with finite-range two-body interactions and no disorder. In contrast to Ref. [22] where the driving protocol involves quenching between two many-body Hamiltonians, which is experimentally challenging, our drive only consists of delta kicks generated by a global magnetic field that periodically applies a $\pi/2$ pulse to each spin.

We find that spin-spin interactions, regardless of their range, help to stabilize the time crystal with a period doubling against small errors in the driving protocol. We analyze the stabilizing mechanism by providing a perturbative model that analyzes the effect of unwanted off-resonant transitions to other undesired states created by errors in the driving protocol. Our setup can be experimentally implemented in all quantum technologies platforms that can realize the quantum Ising model, including trapped ions [26–30], Rydberg atoms [31,32], superconducting circuits [33], and solid state $LiHoF_4$ [34].

II. THE SYSTEM, STATE PREPARATION, AND DRIVING PROTOCOL

We consider the dynamics of the Ising model in a transverse-field described by the Hamiltonian

$$H_0 = -J\sum_i \sigma_i^x \sigma_{i+1}^x - h\sum_i \sigma_i^z \tag{1}$$

under a periodic delta kick in the absence of disorder. Here, σ_i^κ ($\kappa = x, y, z$) is the Pauli matrix operator at site i, h is the strength of the transverse field, and J is the spin-spin coupling strength. The model exhibits a quantum phase transition at $h_c = J$ in the thermodynamic limit. For $h > h_c$, the system's ground state is a quantum paramagnet, while for $h < h_c$, the

*wcyu.physics@gmail.com
†a0122902@u.nus.edu
‡dimitris.angelakis@gmail.com

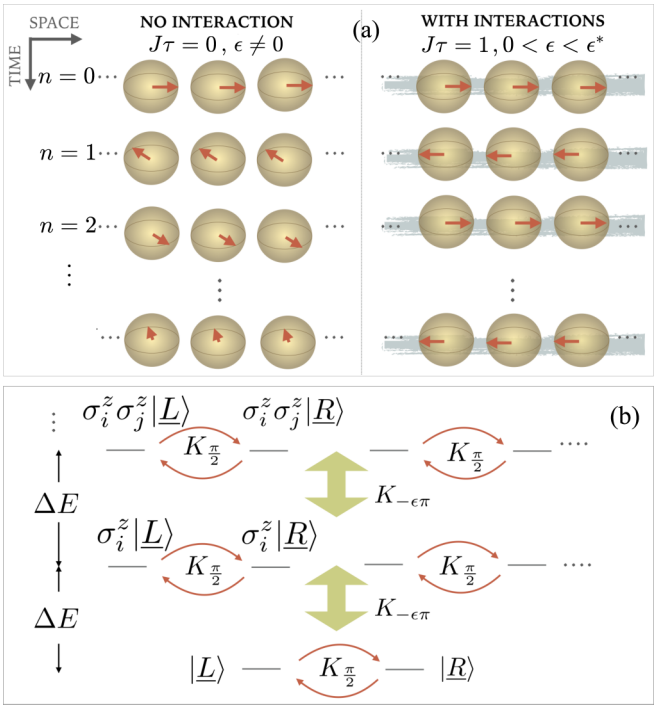

FIG. 1. (a) Schematic diagram showing the dynamics of the individual spins in our model for a small perturbation ϵ in the spin flip. The presence of interaction helps to synchronize the spins. (b) The energy spectrum of the NN Ising model for $h = 0$ and the driving scheme. The energy levels are evenly spaced with a gap $\Delta E = 2J$. The kick operator $K_{\frac{\pi}{2}}$ only connects two eigenstates within the same degenerate manifold, while the errors in the kick operator $K_{-\epsilon\pi}$ may couple different manifolds. However, for the case of off-resonant driving as in our protocol where the driving frequency $\omega_d = 2\pi/\tau$ is far from the energy gap $\Delta E = 2J$, the effect of $K_{-\epsilon\pi}$ is switched off for $\epsilon \ll \epsilon^*$ and the DTC is robust.

system breaks the $\mathbb{Z}_2$ symmetry spontaneously and becomes a ferromagnet [35].

The initial state $|\Psi(0)\rangle$ is prepared in one of the two ferromagnetic ground states of H_0 with $h = 0$. These ground states are simply the product states $|\underline{R}\rangle \equiv \otimes_i|\rightarrow\rangle_i$ and $|\underline{L}\rangle \equiv \otimes_i|\leftarrow\rangle_i$, where $|\rightarrow\rangle_i$ and $|\leftarrow\rangle_i$ are eigenstates of σ_i^x. After evolving the system with H_0 for a time τ, we apply a delta kick

$$K_\phi = \exp\left(-i\phi\sum_i \sigma_i^z\right), \tag{2}$$

which rotates the spins about the z axis by an angle $\phi = \pi(1/2 - \epsilon)$, where ϵ is a perturbation. The procedure is then repeated. The time evolution operator over one period is thus

$$U = K_\phi U_0 = K_{-\epsilon\pi}K_{\pi/2}U_0, \tag{3}$$

where $U_0 = \exp(-iH_0\tau)$ and $\hbar = 1$. For $\epsilon = 0$ and $h = 0$, the kick operator will just flip the spins at every time $n\tau$ and the system returns to the initial state at every 2τ. As will be shown below, the spin-spin interaction in H_0 can "correct" the imperfect spin flip for a small but finite ϵ [Fig. 1(a)], causing the formation of the time crystal [36].

To observe the DTC, we measure the total magnetization in the x direction at every period, i.e.,

$$m^x(n) = \frac{1}{N}\langle\Psi(n)|\sum_i \sigma_i^x|\Psi(n)\rangle, \tag{4}$$

where N is the number of spins in the system and $|\Psi(n)\rangle = U^n|\Psi(0)\rangle$ is the wave function of the system just before the nth kick. We will show that, under an off-resonant driving condition, $m^x(n)$ fulfills the following criteria for the DTC in the thermodynamic limit [22,23]. (1) Time-translational symmetry breaking: $m^x(n+1) \neq m^x(n)$. (2) Rigidity: $m^x(n)$ shows a fixed oscillation period without fine-tuned Hamiltonian parameters. (3) Persistence: the oscillations must persist for infinitely long times. Thus the Fourier transform of $m^x(n)$ has a pronounced peak at π.

III. EFFECTIVE ANALYTIC MODEL

To understand the DTC dynamics in our model, let us first consider the trivial case with $J\tau = h = 0$ where all spins are disconnected and start with an initial state $|\underline{R}\rangle$. The state after n driving periods is simply $|\Psi(n)\rangle = K_\phi^n|\underline{R}\rangle = K_{n\phi}|\underline{R}\rangle$ with the magnetization $m^x(n) = (-1)^n[2\cos^2(\epsilon\pi n) - 1]$. Hence, the Fourier spectrum of $m^x(n)$ has two peaks at $\pi \pm 2\epsilon\pi$, as depicted in Fig. 2(a). This is not a time crystal since the positions of the peaks depend on ϵ regardless of the system size.

When the interaction is switched on ($J\tau \neq 0, h = 0$), the above situation changes dramatically. As will be shown, when the drive is off-resonant, the two main peaks will be separated by a distance proportional to $(\epsilon/\epsilon^*)^{m_a N}$ for a critical value ϵ^* and a positive constant $m_a \sim O(1)$, as depicted in Fig. 2(b). The main peaks' separation will converge to zero as $N \to \infty$ for $\epsilon < \epsilon^*$.

To see this peak merging, let us consider the state after n driving periods $|\Psi(n)\rangle = (K_{\frac{\pi}{2}}K_{-\epsilon\pi}U_0)^n|\underline{R}\rangle$. The driving scheme is depicted in Fig. 1(b). Since $\langle\underline{L}|K_{\frac{\pi}{2}}|\underline{R}\rangle = 1$, the kick operator $K_{\frac{\pi}{2}}$ only flips the two ground states $|\underline{R}\rangle$ and $|\underline{L}\rangle$. It does not connect them to the excited states.

The operator $K_{-\epsilon\pi}$, on the other hand, generates transitions to the excited states. In first order in ϵ, it does not connect the two ground states. We can see this by approximating $K_{-\epsilon\pi}$ to first order in ϵ by $K_{-\epsilon\pi} \approx 1 + i\epsilon\pi\sum_{i=1}^N \sigma_i^z$. Since $K_{-\epsilon\pi}$ only flips one spin, it follows that $\langle\underline{L}|K_{-\epsilon\pi}|\underline{R}\rangle \to 0$ as $\epsilon \to 0$. However, the kick operator couples the ground state to the first excited states $|j\rangle = \sigma_j^z|\underline{R}\rangle$ for $j \in \{1, 2, \ldots N\}$ as $\langle jK_{-\epsilon\pi}\underline{R}\rangle \sim \epsilon$. If the driving frequency $\omega_d = 2\pi/\tau$ is much larger than the energy gap ΔE of H_0, the corresponding transition to the excited states is too far off-resonant to get significantly populated. Hence $K_{-\epsilon\pi}$ is effectively switched off, as will be confirmed by exact diagonalization below.

With the above conditions, the Fourier spectrum of $m^x(n)$, defined as $\widetilde{m^x}(\omega)$, will show a main peak at $\omega\tau = \pi$ and side peaks of height $\sim\epsilon^2$ [37]. When ϵ becomes large, one has to take into account higher order terms in the expansion of $K_{-\epsilon\pi}$. The Nth-order term, in particular, couples the two ground states $|\underline{L}\rangle$ and $|\underline{R}\rangle$, leading to the splitting of the main peak $\delta\omega = |\omega_f\tau - \pi| \approx (\epsilon/\epsilon^*)^{m_a N}$ with $m_a = 1$, and ω_f is the main peak's frequency.

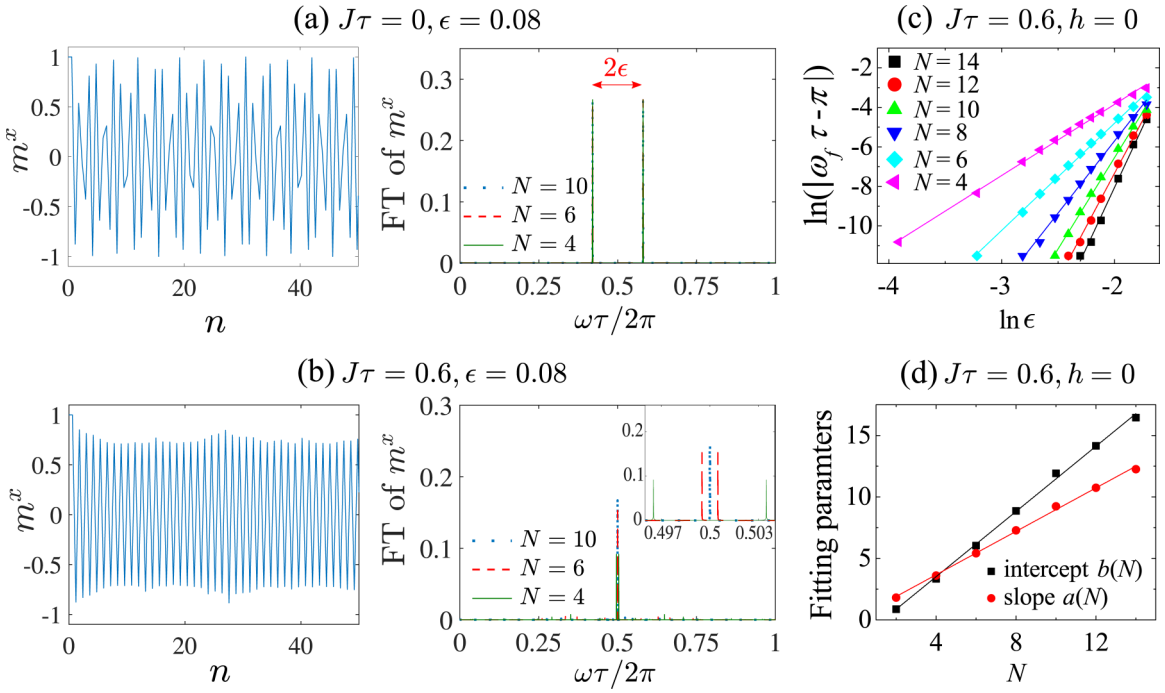

FIG. 2. [(a) and (b)] Stroboscopic magnetization $m^x(n)$ for $N = 10$ and Fourier transforms of $m^x(n)$ for various system sizes N. Here $\epsilon = 0.08$ and $h = 0$. In the absence of spin-spin interaction as shown in (a), the Fourier peaks for various N coincide. The splitting of the two peaks equals 2ϵ for all N while it scales approximately as $(\epsilon/\epsilon^*)^{m_a N}$ from the scaling analysis in (c) and (d) in the presence of interaction. (c) Fourier peak splitting as a function of ϵ for $h = 0, J\tau = 0.6$. The straight lines show the linear fits for various system sizes. (d) The linear fitting parameters of (c) as a function of N. Straight lines show the linear fitting of the data points.

IV. DISCRETE TIME CRYSTAL WITH NEAREST-NEIGHBOR INTERACTIONS

To validate the above picture, we calculate the time evolution using exact diagonalization. The corresponding driving frequency is $\omega_d = 2\pi/\tau \approx 10.5J$, while the energy gap of H_0 is $\Delta E = 2J$. In Fig. 2(c), we plot the splitting $\ln(\delta\omega)$ as a function of $\ln(\epsilon)$ for various system's sizes N. The data for each N is fitted linearly, i.e., $\ln(\delta\omega) = b(N) + a(N)\ln(\epsilon)$. As shown in Fig. 2(d), $a(N)$ and $b(N)$ are approximately linearly dependent on N with the slopes $m_a \approx 0.88$ and $m_b \approx 1.33$, respectively. This linear dependence agrees well with the perturbation theory which predicts $m_a = 1$. In the limit $N \to \infty$, the splitting $\delta\omega \approx (\epsilon/\epsilon^*)^{m_a N}$ goes to zero when $\epsilon < \epsilon^* = \exp(-m_b/m_a) \approx 0.22$ and diverges otherwise.

To analyze the full spectrum including side peaks, in Fig. 3(a), we plot a color map of the Fourier spectrum as a function of ϵ. The spectrum is divided into three regimes: (1) $\epsilon \lesssim 0.14$ where there are two main peaks separated by $(\epsilon/\epsilon^*)^{m_a N}$ around $\omega\tau = \pi$, (2) $0.14 \lesssim \epsilon \lesssim 0.35$ where there is no prominent peak, and (3) $0.35 \lesssim \epsilon < 0.5$ where there is one prominent peak at $\omega = 0$. The corresponding Fourier spectra with values of ϵ taken from each of the regime are shown in Figs. 3(g)–3(i).

To quantify the transitions, we calculate the Kullback-Leibler (KL) divergence defined as [38]

$$\mathrm{KLD} = \sum_{\omega} A_\omega \ln\left(A_\omega/A_\omega^{\mathrm{ref}}\right), \tag{5}$$

where A_ω is the Fourier spectrum of $m^x(n)$ and A_ω^{ref} is the Fourier spectrum of a perfect cosine function with $\omega_f\tau = \pi$ [39]. The sum of the Fourier spectra are normalized to one, i.e., $\sum_\omega A_\omega = \sum_\omega A_\omega^{\mathrm{ref}} = 1$. Physically, the KLD measures how the Fourier spectrum A_ω is different from A_ω^{ref} which signatures a perfect DTC. Figure 3(d) shows the KLD as a function of ϵ. The KLD shows distinct behavior in the three regimes mentioned above, as expected. The dynamics of the three cases can be understood by considering three limiting cases. (1) When $\epsilon = 0$, there is one prominent peak at $\omega\tau = \pi$ as discussed earlier. (2) When $\epsilon = 0.25$, the kick operator rotates $|\underline{R}\rangle$ to $\prod_i(|\rightarrow\rangle_i + |\leftarrow\rangle_i)/\sqrt{2}$, hence maximizing the overlap with the excited states. Thus the Fourier spectrum shows no prominent peak. (3) When $\epsilon = 0.5$, the kick operator is turned off and the state does not evolve. Hence, the Fourier spectrum has a prominent peak at $\omega = 0$.

In Fig. 3(b), we plot the Fourier spectrum as a function of $J\tau$. The spectrum shows five different regimes as $J\tau$ is varied from zero to π. The corresponding transitions, labeled by $J\tau_q^*$ with $q \in \{1, 2, 3, 4\}$, are captured by the KLD, as depicted in Fig. 3(e). These transitions can be understood as follows. In the limit of $J\tau = 0$, as shown in Fig. 2(a), the spectrum displays two main peaks separated by $4\pi\epsilon$. When $J\tau$ is increased, these two peaks create a beating effect where the envelope oscillates over the period τ/ϵ. The kick operator creates excitations that oscillate on the timescale of $2\pi/\Delta E = \pi/J$. The first transition happens when these two timescales become comparable, i.e., $J\tau_1^* = \epsilon\pi \approx 0.4$. This approximated value agrees with the transition shown in Figs. 3(b) and 3(e). As $J\tau_1^* < J\tau < J\tau_2^*$, the drive is off-resonant with ΔE leading to the DTC as discussed earlier. At $J\tau = 0.5\pi$, the drive hits the second harmonic ($\omega_d \sim 2\Delta E$) of the system.

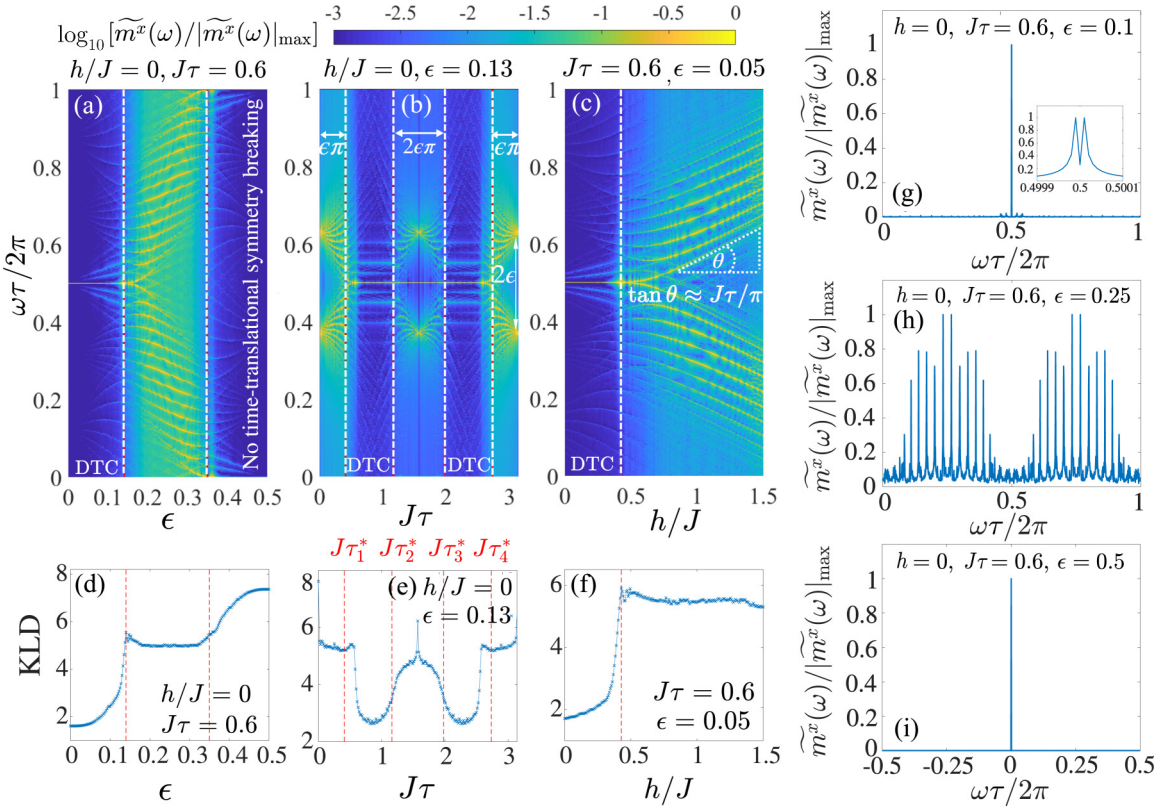

FIG. 3. [(a)–(c)] Color map of the Fourier spectrum of the stroboscopic magnetization in x direction with ϵ, $J\tau$, and h/J as the driving parameter respectively. Here $N = 14$ and the Fourier transform is performed over 1000 periods of the drive. The amplitude of the Fourier peaks is divided by the maximum amplitude for better visualization. [(d)–(f)] KL divergence of the Fourier spectrum in the corresponding upper panel. The plateaus around KLD ~ 2 indicate the DTC phase and the vertical dash lines show the approximated phase boundary. [(g)–(i)] Cuts of the Fourier spectrum color map in (a) for ϵ from three different phases. (g) $\epsilon = 0.1$ and the system is in DTC phase. Inset shows a zoom-in of the main peaks around $\omega\tau = \pi$ (the Fourier transform is carried out over 10^5 periods here). The two main peaks are separated by $(\epsilon/\epsilon^*)^{m_a N}$ in this phase. (h) $\epsilon = 0.25$ and there is no prominent peak observed. (i) $\epsilon = 0.5$ and the system oscillate with the drive. One prominent peak is observed at $\omega = 0$. The spectrum is folded into $[-\pi, \pi)$ for better visualization of the main peak.

In this regime, after two driving periods, the excitations gain the phase of $2\Delta E\tau = 2\pi$. Hence, in the rotating frame that oscillates with the period 2τ, the system will behave as if $J\tau = 0$, leading to two peaks at $\pi \pm 2\epsilon\pi$. When moving back to the original frame that oscillates with the period τ, there is an extra peak at π. The phase boundaries can be calculated as $J\tau_2^* = 0.5\pi - \epsilon\pi$ and $J\tau_3^* = 0.5\pi + \epsilon\pi$. At $J\tau = \pi$, the drive hits the first harmonic of the system. The excitations gain the phase of 2π after one driving period. Hence, the situation is the same as $J\tau = 0$. The phase boundary is $J\tau_4^* = \pi - \epsilon\pi$. At $J\tau_3^* < J\tau < J\tau_4^*$, the drive is off-resonance with the first and the second harmonic of the system, leading to the DTC.

In Fig. 3(c), we plot the Fourier spectrum as a function of h/J. The spectrum shows a transition at $h^*/J \approx 0.5$ which also appears in the corresponding KLD plot in Fig. 3(f). At $h/J > h^*/J$, we observe that the splitting of the main peak grows linearly with h/J with the rate $2\tan\theta \sim 0.40$. This splitting can be understood as follows. In the limit $h/J \gg 1$, the magnetic field dominates the spin-spin interactions and $[U_0, K_\phi] \simeq 0$. Hence, the system evolves with the approximated operator $K_{0.5\pi-\epsilon\pi-h\tau} = K_{\pi(0.5-\epsilon')}$, where $\epsilon' = \epsilon + h\tau/\pi$. Hence the splitting rate is $2\delta\epsilon'/\delta(h/J) = 2\tau/\pi \sim 0.38$ ($J\tau = 0.6$), in agreement with the splitting observed in Fig. 3(c). This relation also holds for other values of $J\tau$ as shown in Fig. 4.

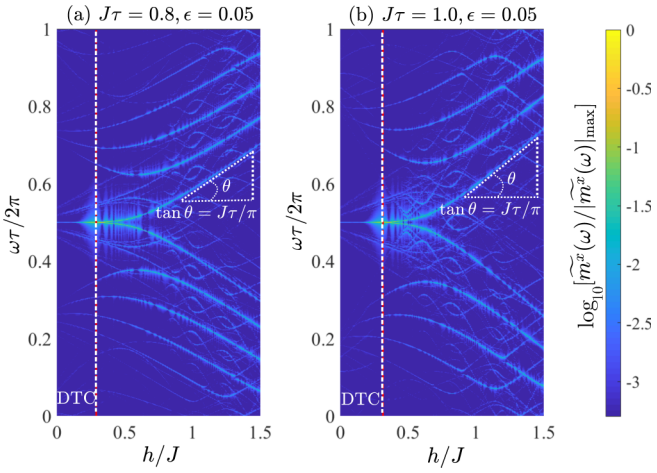

FIG. 4. [(a) and (b)] Color map of the Fourier spectrum of the stroboscopic magnetization in the x direction with h/J as the driving parameter for various $J\tau$. Here, $N = 8$ and the Fourier transform is performed over 1000 periods.

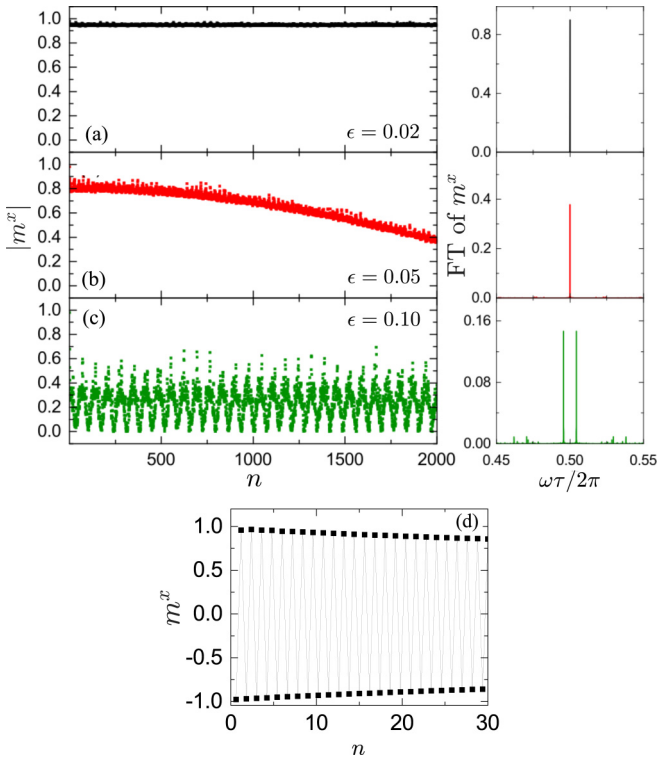

FIG. 5. [(a)–(c)] Stroboscopic magnetization as a function of time for various values of ϵ and the corresponding Fourier spectrum performed over 10^5 kicking periods for $N = 14$, $h/J = 0.32$, and $J\tau = 0.6$. The initial state is prepared in one of ferromagnetic ground states of H_0 with $h/J = 0.32$. (d) Stroboscopic magnetization from TEBD simulation [25] for $N = 80$, $\epsilon = 0.02$, $J\tau = 0.6$, and $h/J = 0.32$. The lines are just guide to the eyes.

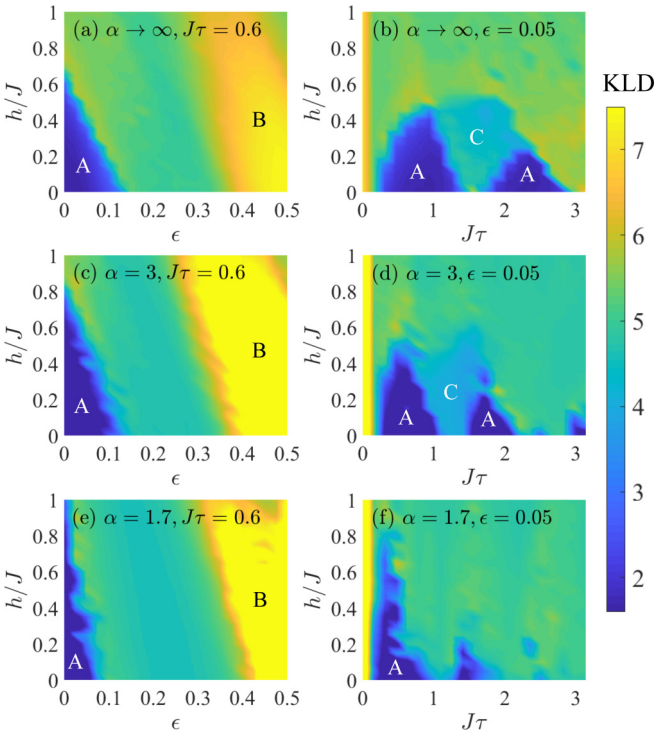

FIG. 6. Color map of the KLD in the $\epsilon - h/J$ and $J\tau - h/J$ parameter space for $N = 14$. The top row corresponds to the nearest-neighbor interacting case ($\alpha \to \infty$) and the interaction range increases down the row. A labels the DTC phase, B labels the regime in which the system oscillates with the drive, and C labels the regime where the drive hits the second harmonic of the system.

We also consider an initial state prepared from one of the ferromagnetic ground states of H_0 in Eq. (1) with $0 < h/J < 1$. In experiment, such a state can be prepared by cooling the system in the presence of a strong magnetic field in the x direction at two ends of the chain. As we can see from Fig. 5, the period doubling in the stroboscopic magnetization remains robust and persists in a large system size [40].

For general values of the driving parameters ϵ, $J\tau$, and h/J, the approximate phase boundaries of DTC are captured by the KLD as shown in Figs. 6(a) and 6(b). The DTC phases are stable up to $h/J \sim 0.6$. For $h/J \neq 0$, the energy spectrum becomes dispersive and bands are formed. In particular, the energy span of the second band increases as h/J increases. This results in the wedgelike shape of phase C in Fig. 6(b). Moreover, the first DTC phase (on the left) is more robust than the second DTC phase (on the right). This is because in order to get out of the first DTC phase, resonance to the states in the second band is required and is more difficult to achieve than populating the states in the first band (which melts the second DTC) since a higher-order perturbation in the kick operator is involved.

V. THE EFFECT OF LONG-RANGE INTERACTIONS

Now let us consider the effect of the range of interaction in stabilizing the DTC. The Hamiltonian is modified to $H_0 = -J\sum_{i<j}\sigma_i^x\sigma_j^x/|i-j|^\alpha - h\sum_i\sigma_i^z$, with α characterizing the interaction range [41,42]. Figures 6(c)–6(f) show the phase diagrams for various values of α in the $(h/J) - \epsilon$ and $(h/J) - J\tau$ planes, respectively. Upon decreasing α (increasing the range of interactions), the DTC phase becomes more robust to the perturbations in the external transverse field (left column of Fig. 6). The long-range interaction helps to maintain the system in the symmetry broken state with a finite magnetization in the x direction as well as stabilizing the DTC against perturbations in the imperfection of the spin flip ϵ. On the other hand, the two DTC phases observed in the nearest-neighbor interacting case in the $J\tau$ parameter space shrink upon introducing long range interactions. To understand this, let us consider the limiting case $h = 0$. In the presence of long-range interactions, spin flips at different sites have different energies. This results in a broadening of the energy spectrum and increasing the probability of populating the excited states. Hence, the stability of the DTC phase decreases.

We further check the stability of the DTC by taking the initial state as one of the ground states of H_0 with $h/J = 0.32$ and introducing noises in the kick by setting ϵ as a random variable, i.e., $K_\phi = \exp[-i\sum_i \phi_i\sigma_i^z]$, where $\phi_i = \pi(1/2 - \epsilon_i)$ and ϵ_i is drawn from a uniform distribution $[0, \epsilon_0]$. The result is shown in Fig. 7. We can see from the left panel of the plot, the period doubling persists for a small ϵ_0 and this further supports the presence of the DTC without fine-tuning

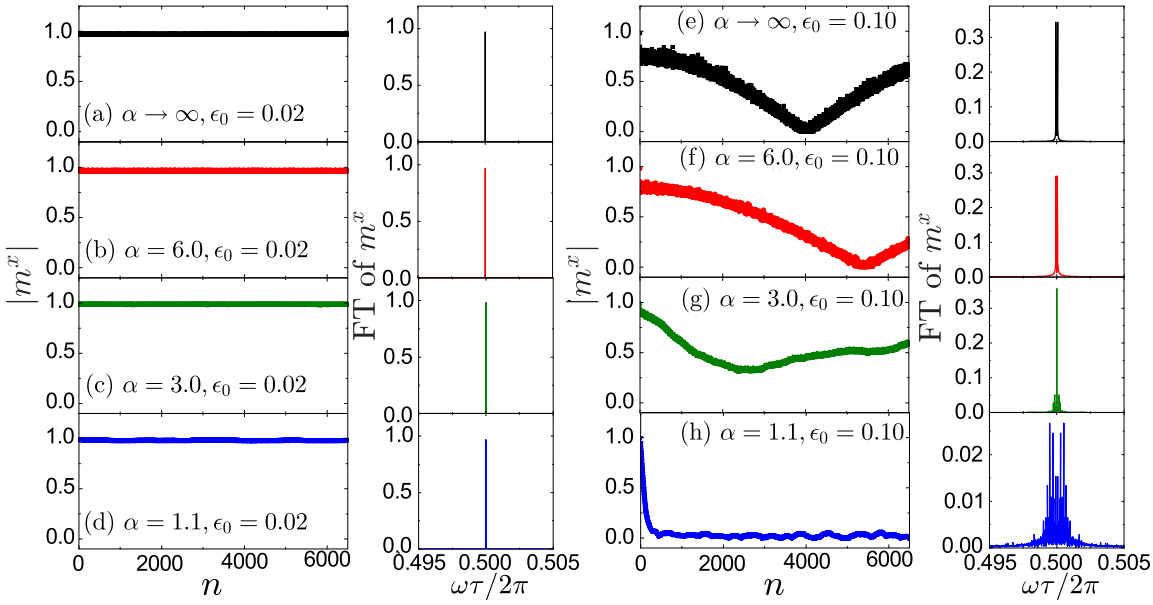

FIG. 7. Stroboscopic magnetization as a function of time and the corresponding Fourier spectrum for various α and ϵ_0. Here, $N = 14$, $h/J = 0.32$, and $J\tau = 0.6$.

the Hamiltonian parameters. As ϵ_0 becomes larger, the DTC becomes less stable and the effect of noise is more pronounce in the case of a smaller α as shown in the right panel of Fig. 7.

VI. CONCLUSIONS

We showed the possibility to observe a stable DTC in an Ising spin system in the absence of disorder subjected only to a periodic drive without the need for any other Hamiltonian control [40]. The simplicity of the global driving protocol should trigger further theoretical and experimental studies in this direction. Among future works, one could consider the effect of the shape of the periodic drive with Gaussian with finite lifetime instead of a delta. The possibility to observe such behavior for different spin Hamiltonians and the dimensionality dependence might be of interest as well.

ACKNOWLEDGMENTS

We thank J.I. Cirac for fruitful discussions and support from the National Research Foundation and the Ministry of Education of Singapore. This research was also partially funded by Polisimulator project co-financed by Greece and the EU Regional Development Fund, the European Research Council under the European Union's Seventh Framework Programme (FP7/2007-2013)/ERC Grant Agreement No. 319286 Q-MAC. D.J. acknowledges support from the EPSRC under Grant Nos. EP/K038311/1, EP/P01058X/1, and EP/P009565/1.

[1] F. Wilczek, Phys. Rev. Lett. **109**, 160401 (2012); see also K. Sacha and J. Zakrzewski, Rep. Prog. Phys **81**, 016401 (2017) for a review.
[2] P. Bruno, Phys. Rev. Lett. **111**, 070402 (2013).
[3] H. Watanabe and M. Oshikawa, Phys. Rev. Lett. **114**, 251603 (2015).
[4] K. Sacha, Phys. Rev. A **91**, 033617 (2015).
[5] V. Khemani, A. Lazarides, R. Moessner, and S. L. Sondhi, Phys. Rev. Lett. **116**, 250401 (2016).
[6] D. V. Else, B. Bauer, and C. Nayak, Phys. Rev. Lett. **117**, 090402 (2016).
[7] C. W. von Keyserlingk, V. Khemani, and S. L. Sondhi, Phys. Rev. B **94**, 085112 (2016).
[8] N. Y. Yao, A. C. Potter, I.-D. Potirniche, and A. Vishwanath, Phys. Rev. Lett. **118**, 030401 (2017).
[9] A. Lazarides and R. Moessner, Phys. Rev. B **95**, 195135 (2017).
[10] M. Mierzejewski, K. Giergiel, and K. Sacha, Phys. Rev. B **96**, 140201(R) (2017).
[11] J. Zhang, P. W. Hess, A. Kyprianidis, P. Becker, A. Lee, J. Smith, G. Pagano, I. D. Potirniche, A. C. Potter, A. Vishwanath, N. Y. Yao, and C. Monroe, Nature (London) **543**, 217 (2017).
[12] J. Rovny, R. L. Blum, and S. E. Barrett, Phys. Rev. Lett. **120**, 180603 (2018).
[13] J. Rovny, R. L. Blum, and S. E. Barrett, Phys. Rev. B **97**, 184301 (2018).
[14] S. Choi, J. Choi, R. Landig, G. Kucsko, H. Zhou, J. Isoya, F. Jelezko, S. Onoda, H. Sumiya, V. Khemani, C. von Keyserlingk, N. Y. Yao, E. Demler, and M. D. Lukin, Nature (London) **543**, 221 (2017).
[15] W. W. Ho, S. Choi, M. D. Lukin, and D. A. Abanin, Phys. Rev. Lett. **119**, 010602 (2017).
[16] D. A. Abanin, W. De Roeck, W. W. Ho, and F. Huveneers, Phys. Rev. B **95**, 014112 (2017).

[17] G. Kucsko, S. Choi, J. Choi, P. C. Maurer, H. Zhou, R. Landig, H. Sumiya, S. Onoda, J. Isoya, F. Jelezko, E. Demler, N. Y. Yao, and M. D. Lukin, Phys. Rev. Lett. **121**, 023601 (2018).
[18] T. S. Zeng and D. N. Sheng, Phy. Rev. B **96**, 094202 (2017).
[19] D. V. Else, B. Bauer, and C. Nayak, Phys. Rev. X **7**, 011026 (2017).
[20] A. Russomanno, B.-E. Friedman, and E. G. Dalla Torre, Phys. Rev. B **96**, 045422 (2017).
[21] S. Pal, N. Nishad, T. S. Mahesh, and G. J. Sreejith, Phys. Rev. Lett. **120**, 180602 (2018).
[22] B. Huang, Y. H. Wu, and W. V. Liu, Phy. Rev. Lett. **120**, 110603 (2018).
[23] A. Russomanno, F. Iemini, M. Dalmonte, and R. Fazio, Phys. Rev. B **95**, 214307 (2017).
[24] K. Giergiel, A. Kosior, P. Hannaford, and K. Sacha, Phys. Rev. A **98**, 013613 (2018).
[25] S. Al-Assam, S. R. Clark, and D. Jaksch, J. Stat. Mech. (2017) 093102.
[26] J. W. Britton, B. C. Sawyer, A. C. Keith, C. C. J. Wang, J. K. Freericks, H. Uys, M. J. Biercuk, and J. J. Bollinger, Nature **484**, 489 (2012).
[27] R. Islam, C. Senkol, W. C. Campbell, S. Korenblit, J. Smith, A. Lee, E. E. Edwards, C. C. J. Wang, J. K. Freericks, and C. Monroe, Science **340**, 583 (2013).
[28] P. Richerme, Z.-X. Gong, A. Lee, C. Senko, J. Smith, M. Foss-Feig, S. Michalakis, A. V. Gorshkov, and C. Monroe, Nature **511**, 198 (2014).
[29] P. Jurcevic, B. P. Lanyon, P. Hauke, C. Hempel, P. Zoller, R. Blatt, and C. F. Roos, Nature **511**, 202 (2014).
[30] J. G. Bohnet, B. C. Sawyer, J. W. Britton, M. L. Wall, A. M. Rey, M. Foss-Feig, and J. J. Bollinger, Science **352**, 1297 (2016).
[31] H. Labuhn, D. Barredo, S. Ravets, S. de Léséleuc, T. Macrì, T. Lahaye, and A. Browæys, Nature **534**, 667 (2016).
[32] J. Zeiher, J.-Y. Choi, A. Rubio-Abadal, T. Pohl, R. van Bijnen, I. Bloch, and C. Gross, Phys. Rev. X **7**, 041063 (2017).
[33] S. Boixo, T. F. Rønnow, S. V. Isakov, Z. Wang, D. Wecker, D. A. Lidar, J. M. Martinis, and M. Troyer, Nat. Phys. **10**, 218 (2014).
[34] D. M. Silevitch, G. Aeppli, and T. F. Rosenbaum, Proc. Natl. Acad. Sci. USA **107**, 2797 (2010).
[35] S. Sachdev, *Quantum Phase Transitions* (Cambridge University Press, Cambridge, UK, 2000).
[36] A similar kicking protocol has been used for the infinite range in the Lipkin-Meshkov-Glick (LMG) model [23].
[37] See Supplemental Material at http://link.aps.org/supplemental/10.1103/PhysRevA.99.033618 for an analytical form of the magnetization derived from first-order perturbation theory.
[38] S. Kullback and R. A. Leibler, Ann. Math. Statist. **22**, 79 (1951).
[39] A small noise of order 10^{-5} is added to $A_{\omega}^{\mathrm{ref}}$ to avoid divergence caused by a zero in the denominator in Eq. (5).
[40] In Supplemental Material, the eigenspectrum of the unitary operator in Eq. (3) and the π-spectral pairing [7,6,5,23] are also analyzed.
[41] D. Jaschke, K. Maeda, J. D. Whalen, M. L. Wall, and L. D. Carr, New J. Phys. **19**, 033032 (2017).
[42] Z. Zhu, G. Sun, W. L. You, and D. N. Shi, Phys. Rev. A **98**, 023607 (2018).